International Journal of Control, Automation, and Systems (2010) 8(6):1271-1279 http://www.springer.com/12555
DOI 10.1007/s12555-010-0612-y

Dynamics and Stabilization of a Spherical Inverted Pendulum on a Wheeled Cart

Myung-Gon Yoon

Abstract: This paper studies a stabilization problem of an inverted spherical pendulum on a wheeled cart assuming that pure rotation of cart cannot move support of pendulum. It is shown that in spite of nonholonomic constraints of wheels and the above geometric condition on pendulum support the pendulum can be locally stabilizable at a certain non-static equilibrium point by applying a standard linearization approach. Furthermore it is shown that equilibrium points can be chosen to make cart move to a given location. Numerical simulations are performed to confirm theoretical findings and illustrate interesting dynamics of closed loop pendulum system.

Keywords: Linearization, nonholonomic constraints, spherical inverted pendulum.

1. INTRODUCTION

Doubtlessly the inverted pendulum is one of the most famous control system that can be found in most textbooks for introductory control course and many control laboratories worldwide. This popularity seems to come from the fact that one can intuitively see control actions even though a simple mechanical system. Moreover inverted pendulums can show both linear and nonlinear behaviors, depending on desired motions such as the swing-up and employed control algorithms. This is why many newly proposed controller algorithms have been testified with some kind of inverted pendulum.

Spherical or three dimensional (3D), confusingly two dimensional (2D) in some literature, inverted pendulum often appeared as academic examples in mathematically oriented nonlinear control methodologies, e.g., see recent papers [1,2] for examples. The pendulum dynamics in those papers is relatively simple as the dynamics and any constraints of cart supporting the pendulum are not practically considered. In fact it is well known and experimentally verified that if the cart can freely move on a plane without any constraints then the spherical pendulum can be easily stabilized by applying two decoupled linear controllers for each coordinate [3].

On the other hand pendulum-type wheeled robots attracted much attention in robotics area and various kinds of such balancing robots has been implemented [4-7]. In those works a robot body is modeled as an inverted pendulum on a supporting body with wheels that will be called as a general name *cart* in this paper. A key issue was how to steer the robot to a desired location while stabilizing the pendulum subject to the nonholonomic constraints of driving wheels, i.e., the no-slip condition. Note that the robot body, which is a pendulum, of the above studies was mechanically constrained to have only one degree of rotational freedom or the pitch motion. In other words, if the cart is fixed to the ground, then the robot body becomes a standard one-dimensional inverted pendulum.

As a generalization we will consider a spherical inverted pendulum on a wheeled cart in this paper. In addition to the no-slip constraint of wheels we assume that pure rotational motion of cart will not induce any planar motions of the joint supporting pendulum. Though not explicit, this geometric constraint on pendulum support is satisfied in many pendulum-type wheeled robots considered in [5-7]. As will be explained later, without that constraint, our generalization from one-dimensional pendulum to spherical one on a wheeled cart becomes less challenging as existing linearization technique and coordinate decoupling still work without any intrinsic performance limitations.

Within the author's knowledge, spherical inverted pendulum on a wheeled cart has never studied in literature. However, for a claim of its importance, we note that in the case of existing pendulum-type wheeled robots the rotation of body upon the traveling direction, or the roll motion, is suppressed by a reaction torque at a joint mechanism connecting body to wheels. That torque however can make robot wheels loose contact with the ground and possibly cause a turnover in the worst case. As no torques can arise in our spherical pendulum model, our investigations in this paper will provide useful insights on how to avoid those undesirable situations. Moreover from practical viewpoint we mention that the commercial transportation equipment *Segway*©, for an example, is closer to our model than existing one-dimensional balancing robots as its pendulum, a rider in this case, can lean to the left or right [8]. Similarly it is

Manuscript received February 5, 2010; revised June 8, 2010; accepted August 2, 2010. Recommended by Editorial Board member Youngjin Choi under the direction of Editor Jae-Bok Song. This work was supported by the Grant for the Promotion of Research 2005 by Gangneung-Wonju National University. Preliminary study was supported by the Australian Research Council and Australian Defence Science and Technology Organisation in 2003.

Myung-Gon Yoon is with the Department of Precision Mechanical Engineering, Gangneung-Wonju National University, Gangneung 120-702, Korea (e-mail: mgyoon@gwnu.ac.kr).

more reasonable to model a humanoid robot as a spherical pendulum than a one-dimensional one as done in [5].

A standard linearization technique will be employed in this paper. We will firstly derive nonlinear dynamic equations of our spherical pendulum and then investigate an equilibrium manifold on which a linearized model can be found. With this linearized model it will be shown that the pendulum can be locally controllable in some loose sense and globally steerable by choosing a suitable operating point. During those developments, as being a linearization approach essentially, our focus will be not on specific controllers but the interesting pendulum dynamics arising from both the nonholonomic and geometric constraints, and performance limitations of closed loop pendulum system.

2. PENDULUM SYSTEM AND PROBLEM DEFINITION

A schematic of a spherical inverted pendulum system under our consideration is shown in Fig. 1. Implicitly we assume that the lower end, point *B*, of pendulum, call it pendulum support or support in short, is connected at the center of the wheel axis (a line connection the centers of two wheels) denoted by *C*, which explains the symbol *B*=*C* therein. Even though we will be addressing only the case *B*=*C* for simplicity in the following developments, a geometric constraint imposed on the pendulum system can be generally stated as follows;

Assumption 1: Both the pendulum support and the center of wheel axis have the same projection on the ground. Equivalently, pure rotation of cart will not cause any planar movements of the pendulum support.

The symbol "4" on the cart body in Fig. 1 defines the forward direction of the cart. With this symbol the rotational displacements of right and left wheels denoted θ_r and θ_l are unambiguously identified. For a description of pendulum gesture we introduced a fictitious instantaneous hexahedron (dashed) and two solid diagonal lines on it. Then the position of pendulum can be uniquely given by signed quantities α and β. For instance the pendulum shown in Fig. 1 has $\alpha > 0$ and $\beta > 0$. For simplicity we assume that the mass center of the cart also coincides with the point *B*=*C* and represent the global position of cart by a planar point (*x*, *y*) and an angle $\phi \in [-\pi, \pi)$. Note that the angle ϕ is defined by the forward direction of the cart. Our pendulum system shown in Fig. 1 has the following physical parameters;

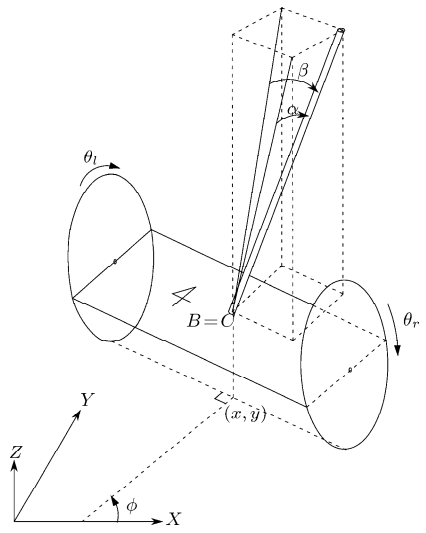

Fig. 1. Schematic of spherical inverted pendulum.

- m_c, m: mass of cart (with wheels) and pendulum, respectively.
- ℓ, r: length of pendulum and wheel radius, respectively.
- *b*: half of the distance between two wheels.
- J_ϕ: moment of inertia of cart with respect to the *Z*-axis, excluding the pendulum.
- J_w: moment of inertia of wheel with respect to the wheel axis.
- *g*: gravitational acceleration constant.

Up to now we have addressed seven variables $\{\theta_r, \theta_\ell, \alpha, \beta, x, y, \phi\}$ to describe a configurations of pendulum but from the *holonomic* constraint $\dot{\phi} = \frac{r}{2b}(\dot{\theta}_r - \dot{\theta}_l)$ three variables $\{\theta_l, \theta_r, \phi\}$ can be reduced to two. Instead of removing one however we introduce a new variable $s := \frac{r}{2}(\theta_r + \theta_l)$ and will replace the three variables $\{\theta_l, \theta_r, \phi\}$ by the two variables $\{\phi, s\}$.

The pendulum system also has the following *no-slip* (nonholonomic) conditions

$$\dot{x}\sin\phi - \dot{y}\cos\phi = 0, \tag{1}$$

$$\dot{x}\cos\phi + \dot{y}\sin\phi = \dot{s}. \tag{2}$$

As these will not reduce the number of minimal variables, we choose $\{q_j\} := \{x, y, s, \phi, \alpha, \beta\}$ as the configuration variables of our pendulum system. Now assuming that torque inputs $\{\tau_r, \tau_l\}$ at wheels are independent control inputs, we can formally state our stabilization problem as follows;

Problem 1: *Given small initial angles, is it possible to stabilize the pendulum with linear controllers under the Assumption 1?*

Here by *linear controllers* we mean a standard combination of plant linearization and linear controller synthesis.

Quick reasoning might reveal that the above problem is not trivial. Let us suppose the pendulum in Fig. 1 initially leans to the right side of cart, i.e., $\alpha = 0$, $\beta > 0$. Then from our experiences in *local* stabilization of standard inverted pendulum it is expected to somehow move the pendulum support, the point *B*, to the right of cart for stabilization. That motion however is prohibited from Assumption 1 and the wheel's nonholonomic

constraints. Thus Problem 1 requires more than our familiar strategy for classical inverted pendulums. On the other hand the formidable complexity in pendulum dynamics to be shown below makes it hardly promising to apply existing nonlinear control methodologies for a complete answer to Problem 1.

3. MAIN RESULTS

3.1. Dynamic model of pendulum system

Basically the nonlinear dynamic model presented in this paper is obtained from a routine application of the *Lagrange-d'Alembert equations*.

In order to make a linearization process easy however we have derived a normal form, i.e., a holonomic system equivalent to a nonholonomic system with some simplifications specific to our pendulum system instead of following general procedures described in [9]. A short description on the derivation of nonlinear model can be found in Appendix.

Our calculations give the following nonlinear model;

$$M(\alpha,\beta)[\ddot{s}\ \ddot{\alpha}\ \ddot{\phi}\ \ddot{\beta}]^t + C(\dot{s},\dot{\alpha},\dot{\phi},\dot{\beta},\alpha,\beta) = F[u_s\ u_\phi]^t, \quad (3)$$

where the matrices M, C, F are given in (4)-(6).

In general a linearization of a nonholonomic system is much more sophisticated compared to that of holonomic systems. A key difficulty is how to properly merge nonholonomic constraints into a linearization process. In order to make this procedure easy, we have already obtained a normal form (3) and slightly modified the linearization procedure of [10] in favor of a reduced number of states.

As a first step let us note that both $M(\alpha,\beta)$ and $C(\dot{s},\dot{\alpha},\dot{\phi},\dot{\beta},\alpha,\beta)$ in (3) do not explicitly depend on the variable $\{s,\phi\}$ and thus the pendulum dynamics is invariant with respect to those variables, even though the nonholonomic constraint (1)-(2) does depend on the variable ϕ. From this observation we choose the following state vector

$$p := \left[\dot{s}\ \ \dot{\alpha}\ \ \dot{\phi}\ \ \dot{\beta}\ \ \alpha\ \ \beta\right] \quad (7)$$

for a linearized model and by doing so the total number of states is reduced from eight in (3) to six.

$$M(\alpha,\beta) := \begin{bmatrix} \frac{6(m+m_c+2m_w)}{m\ell} & 3\cos\alpha & 3\sin\beta & 0 \\ 3\cos\alpha & \frac{\ell(1+\cos 2\alpha)(1+\cos 2\beta)}{\cos 2\alpha+\cos 2\beta} & 2\ell\cos\alpha\sin\beta & \frac{\ell\sin 2\alpha\sin 2\beta}{\cos 2\alpha+\cos 2\beta} \\ 3\sin\beta & 2\ell\cos\alpha\sin\beta & \ell(2-\cos 2\alpha-\cos 2\beta+\frac{6\tilde{J}_\phi}{m\ell^2}) & -2\ell\sin\alpha\cos\beta \\ 0 & \frac{\ell\sin 2\alpha\sin 2\beta}{\cos 2\alpha+\cos 2\beta} & -2\ell\sin\alpha\cos\beta & \frac{\ell(1+\cos 2\alpha)(1+\cos 2\beta)}{\cos 2\alpha+\cos 2\beta} \end{bmatrix}, \quad (4)$$

$$C(\dot{s},\dot{\alpha},\dot{\phi},\dot{\beta},\alpha,\beta) := \begin{bmatrix} -3\sin\alpha(\dot{\alpha}^2+\dot{\phi}^2)+6\cos\beta\dot{\beta}\dot{\phi} \\ -\ell\sin 2\alpha\dot{\phi}^2+\frac{\ell\sin 2\alpha\sin^2 2\beta}{(\cos 2\alpha+\cos 2\beta)^2}\dot{\alpha}^2+\frac{\ell(4\cos 2\alpha\cos 2\beta+\cos 4\beta+3)\sin 2\alpha}{2(\cos 2\alpha+\cos 2\beta)^2}\dot{\beta}^2 \\ \quad +\frac{2\ell\sin^2 2\alpha\sin 2\beta}{(\cos 2\alpha+\cos 2\beta)^2}\dot{\alpha}\dot{\beta}+4\ell\cos\alpha\cos\beta\dot{\beta}\dot{\phi}-\frac{3\sin 2\alpha}{\sqrt{2}\sqrt{\cos 2\alpha+\cos 2\beta}}g \\ 2\ell\sin\alpha\sin\beta(\dot{\beta}^2-\dot{\alpha}^2)+3\sin\alpha\dot{s}\dot{\phi}+2\ell(\sin 2\beta\dot{\beta}+\sin 2\alpha\dot{\alpha})\dot{\phi} \\ -\ell\sin 2\beta\dot{\phi}^2+\frac{\ell\sin^2 2\alpha\sin 2\beta}{(\cos 2\alpha+\cos 2\beta)^2}\dot{\beta}^2+\frac{\ell(4\cos 2\alpha\cos 2\beta+\cos 4\alpha+3)\sin 2\beta}{2(\cos 2\alpha+\cos 2\beta)^2}\dot{\alpha}^2 \\ \quad +\frac{2\ell\sin 2\alpha\sin^2 2\beta}{(\cos 2\alpha+\cos 2\beta)^2}\dot{\alpha}\dot{\beta}-4\ell\cos\alpha\cos\beta\dot{\alpha}\dot{\phi}-\frac{3\sin 2\beta}{\sqrt{2}\sqrt{\cos 2\alpha+\cos 2\beta}}g \\ -3\cos\beta\dot{s}\dot{\phi} \end{bmatrix}, \quad (5)$$

$$F = \frac{6}{m\ell}\begin{bmatrix} 1 & 0 \\ 0 & 0 \\ 0 & 1 \\ 0 & 0 \end{bmatrix}, \qquad \begin{bmatrix} u_s \\ u_\phi \end{bmatrix} := \begin{bmatrix} (\tau_r+\tau_l)/r \\ b(\tau_r-\tau_l)/r \end{bmatrix}, \qquad \tilde{J}_\phi := J_\phi + m_w b^2, \qquad m_w := 2J_w/r^2. \quad (6)$$

Fact 1: The equality $C(v_e,0,\omega_e,0,0,\beta_e)=0$ holds if three parameters (v_e,ω_e,β_e) satisfy the following equation

$$3v_e\omega_e\cos\beta_e+(2\ell\omega_e^2\cos\beta_e+3g)\sin\beta_e=0. \tag{8}$$

This observation reveals that the next two dimensional manifold in three dimensional Euclidean space

$$\begin{aligned}\Omega:=\{(v_e,\omega_e,\beta_e);&3v_e\omega_e\cos\beta_e\\&+(2\ell\omega_e^2\cos\beta_e+3g)\sin\beta_e=0\}\subset\mathbb{R}^3\end{aligned} \tag{9}$$

can be seen as an equilibrium set of the nonlinear model (3) when $u=0$ by associating the point $(v_e,\omega_e,\beta_e)\in\Omega$ with an equilibrium state $p_e:=[\,v_e\ \ 0\ \ \omega_e\ \ 0\ \ 0\ \ \beta_e\,]$. Therefore the nonlinear pendulum model (3) can be linearized at a given p_e as follows;

$$\begin{aligned}&[\ddot{s}\ \ \ddot{\alpha}\ \ \ddot{\phi}\ \ \ddot{\beta}]^T=[\delta\ddot{s}\ \ \delta\ddot{\alpha}\ \ \delta\ddot{\phi}\ \ \delta\ddot{\beta}]^T\\&=-M(0,\beta_e)^{-1}\left[C(p_e)+\left.\frac{\partial C}{\partial p}\right|_{p_e}\delta p\right]+M(0,\beta_e)^{-1}Fu\\&=-\left(M(0,\beta_e)^{-1}\frac{\partial C}{\partial p}\right)\Big|_{p_e}\delta p+M(0,\beta_e)^{-1}F\Big|_{p_e}u,\end{aligned} \tag{10}$$

where $p:=p_e+\delta p$ and δp denotes a perturbation $\delta p:=[\delta s\ \ \delta\dot{\alpha}\ \ \delta\dot{\phi}\ \ \delta\dot{\beta}\ \ \delta\alpha\ \ \delta\beta]$. This yields the following linearized pendulum model

$$\delta\dot{p}=A(v_e,\omega_e,\beta_e)\delta p+B(\beta_e)u, \tag{11}$$

where the matrices A, B are given in (12)-(13).

Fact 2: From the following linear approximation of the condition (8)

$$3v_e\omega_e+(2\ell\omega_e^2+3g)\beta_e=0, \tag{14}$$

it follows that the (3,5) -th element of the matrix A is zero, i.e., $A(3,5)=0$ in (12).

3.2. Local stabilization of pendulum

First of all let us clarify a physical meaning of the equilibrium condition (8) with a schematic of pendulum in Fig. 2 where the signed real number R_e^{-1} denotes the instantaneous radius of curvature of the path along which the cart runs.

A differential mass dm of pendulum in Fig. 2 is subject to both gravitation force $dF_g:=g\,dm$ and centrifugal force $dF_c:=(R_e+\zeta\sin\beta_e)\omega_e^2\,dm$ with a coordinate variable $\zeta\in[0,\ell]$. A summation of torques in the direction of the velocity v_e induced by those two forces over the whole pendulum, call it M_p, can be calculated as

$$\begin{aligned}M_p&:=\int_0^\ell(\zeta\sin\beta_e dF_g+\zeta\cos\beta_e dF_c)\\&=\frac{m\ell}{6}[3v_e\omega_e\cos\beta_e+(3g+2\ell\omega_e^2\cos\beta_e)\sin\beta_e],\end{aligned} \tag{15}$$

where $\rho:=m/\ell$, $d\zeta=dm/\rho$ and we have used the relation $R_e=v_e/\omega_e$ $(\omega_e\neq0)$.

As the expression inside the bracket of (15) is nothing

$$A(v_e,\omega_e,\beta_e)=\begin{pmatrix}0&0&0&0&-\frac{3mg}{\tilde{m}_1}&0\\0&0&0&-2\omega_e&\frac{6g\tilde{m}_2}{\tilde{m}_1\ell}+\frac{3m\ell\beta_e(v_e\omega_e\tilde{m}_1-3g\beta_e m)}{\tilde{m}_1\tilde{J}_\phi}+\omega_e^2&0\\0&0&0&0&-\frac{m\ell(3v_e\omega_e+2\beta_e\ell\omega_e^2+3\beta_e g)}{\tilde{J}_\phi}&0\\\frac{3\omega_e}{2\ell}&\frac{3v_e}{2\ell}+2\beta_e\omega_e&2\omega_e&0&0&\frac{2\ell\omega_e^2-3\beta_e v_e\omega_e+3g}{2\ell}\\0&1&0&0&0&0\\0&0&0&1&0&0\end{pmatrix}, \tag{12}$$

$$B(\beta_e)=\begin{pmatrix}\frac{4}{\tilde{m}_1}&0\\-\frac{6}{\tilde{m}_1\ell}&-\frac{6\beta_e}{\tilde{J}_\phi}\\0&\frac{6}{\tilde{J}_\phi}\\0&0\\0&0\\0&0\end{pmatrix},\quad \tilde{m}_1:=m+4m_c+8m_w,\quad \tilde{m}_2:=m+m_c+2m_w. \tag{13}$$

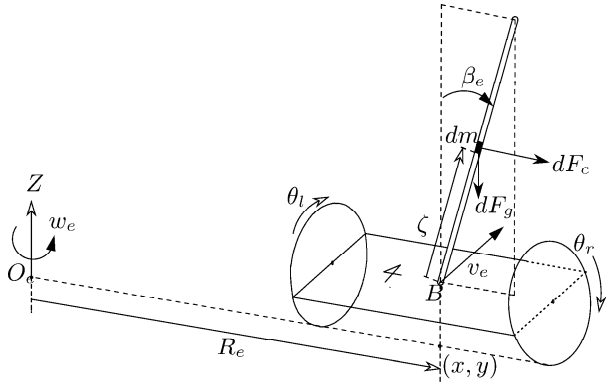

Fig. 2. Schematic of an equilibrium motion.

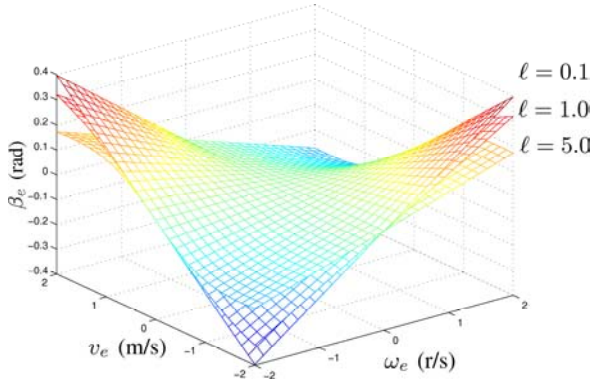

Fig. 3. Equilibrium manifolds.

but the left hand side of the equilibrium condition (8) we obtain the following result;

Fact 3: The inclusion $(v_e, \omega_e, \beta_e) \in \Omega$ holds if and only if the net torques acting on pendulum from both gravitational and centrifugal forces is zero.

As the pendulum support cannot instantly move in the direction of $\pm R_e$ in Fig. 2 by any motions of wheels, regarding the pendulum as a one-dimensional inverted pendulum swinging in the direction of $\pm R_e$, Fact 3 reveals that the centrifugal force is an essential component for stabilizing the pendulum.

Lemma 1: If $(v_e, \omega_e, \beta_e) \in \Omega$, then $\beta_e = 0$ if and only if $v_e \omega_e = 0$.

Proof: This claim follows from the condition (8) with elementary reasoning. For the sufficiency part of the case $v_e = 0$, $\omega_e \neq 0$ note that $(2\ell\omega_e^2 \cos\beta_e + 3g) > 3g > 0$ for $|\beta_e| < \pi/2$.

This lemma shows that if one chooses a perfectly upright pendulum as an equilibrium point then the condition (8) requires $v_e \omega_e = 0$ and thus there are three possibilities; (i) the cart purely rotates around a fixed point B $(\omega_e \neq 0, v = 0)$, (ii) the cart moves rectilinearly $(\omega_e = 0, v_e \neq 0)$ and (iii) the cart is at rest $(\omega_e = v_e = 0)$. The last case corresponds to the standard static equilibrium point which cannot be chosen in our pendulum system from the following fact.

Lemma 2: The linearized plant (11) is not controllable if $(v_e, \omega_e, \beta_e) = (0,0,0)$.

Proof: All components of the matrix A, except $\{A(1,5), A(2,5), A(4,6), A(5,2), A(6,4)\}$, are zero if $(v_e, \omega_e, \beta_e) = (0,0,0)$ holds and thus the rank of controllability matrix $[B \;\; AB \cdots A^5 B]$ becomes four.

This result reveals that there is a fundamental limitation in applying standard linearization techniques to our pendulum in the sense that the static equilibrium, that is, a perfectly upright pendulum on a motionless cart, is not a feasible equilibrium point. This consequence comes from a combination of the geometric condition in Assumption 1 and the no-slip condition of wheels.

In fact our derivations of a linearized model can be easily generalized after removing Assumption 1 and then the resulting linear model at static equilibrium point $(v_e, \omega_e, \beta_e) = (0,0,0)$ becomes controllable as expected from the fact that a pure cart rotation can move the pendulum support in the direction of $\pm R_e$, even under the nonholonomic constraint.

A geometric shape of equilibrium manifold Ω in three dimensional space is shown in Fig. 3 where we have used the linearized equilibrium condition (14) with three different pendulum length $\ell = 0.1$, 1,5. As $0 \in \Omega$ and the equilibrium manifold is smooth, it is clear that one can choose operating points arbitrarily close to the origin even though the origin itself is not feasible. In other words a linear controller can provide an almost upright pendulum $(\beta_e \approx 0)$ on a cart of arbitrarily slow speed $(v_e \approx \omega_e \approx 0)$, provided that initial configuration of pendulum system is sufficiently close to the chosen operating point $(\beta_e, v_e, \omega_w) \approx 0$, which serves as our partial answer to the Problem 1.

3.3. Steering of cart

In this section we propose a way to choose an equilibrium point (β_e, v_e, ω_e) for the purpose of steering pendulum cart to a given destination $r_f := (x_f, y_f)$, assuming that a local controller designed for that particular equilibrium point is stabilizing pendulum. Our idea is motivated from the classical *pure proportional navigation (PPN)* law in missile guidance field, e.g., see [11].

In order to show similarities between our steering problem and a missile guidance problem, choosing $(x_f, y_f) = (0,0)$ without losing generality, let us rewrite the nonholonomic constraints (1)-(2) as

$$\dot{x} = \dot{s}\cos\phi, \quad \dot{y} = \dot{s}\sin\phi, \tag{16}$$

where $\phi = \arg([\dot{x} \;\; \dot{y}])$ and $\arg(\cdot) \in [-\pi, \pi)$ denotes an argument of a vector. These equations, combined with the following third equation,

$$u_{acc} = \dot{s}\dot{\phi} \tag{17}$$

describe trajectory (x, y) of a missile of constant tangential speed $\dot{s}$ and acceleration command u_{acc}.

The following special form of acceleration command

$$u_{acc} = N\dot{s}\dot{\sigma}, \quad \sigma := \arg([x \;\; y]) \tag{18}$$

for some constant $N>1$, is called as the PPN law. Comparing (17) with (18), it follows that

$$\dot{\phi} = N\dot{\sigma} = N\dot{s}\mu, \quad \mu := \frac{\sin(\phi - \sigma)}{\sqrt{x^2 + y^2}}. \tag{19}$$

It is a standard result that when $N=2$ the PPN law makes missile move on a circular path to the origin and thus each of $\{\dot{\sigma}, \dot{\phi}, \mu\}$ is constant.

A connection between the guidance and our steering problem is that the equilibrium parameters (ω_e, v_e) of our pendulum correspond to $\{\dot{\phi}, \dot{s}\}$ in the above PPN law. Thus the PPN law with $N=2$ can be implemented for the pendulum by taking

$$w_e = 2 v_e \mu. \tag{20}$$

Note that, given one parameter among $\{v_e, \omega_e, \beta_e\}$, this equation and the equilibrium condition (8) uniquely determine the other two and thus an equilibrium point $p_e = (v_e, \omega_e, \beta_e) \in \Omega$. With this particular choice of equilibrium point, according to the above results of the PPN law, it is guaranteed that cart will approach to the origin on a circular path.

From this choice of equilibrium point and an application of the previous linearization technique, in spite of both the geometric and nonholonomic constraints, our pendulum can be stabilized in some *weak* sense that cart can be steered to a desirable destination with a nearly upright pendulum.

From theoretical viewpoint however our result has a fundamental limitation that global stability of closed loop pendulum system cannot be analytically substantiated from the linearization process involved.

4. A NUMERICAL EXAMPLE

This section presents a numerical example of closed loop pendulum system combined with a linear stabilizing controller based on a PPN-motivated equilibrium point.

Our focus here is not to claim some level of closed loop performance, but to numerically verify our developments up to now and to illustrate interesting closed loop pendulum dynamics even with a simple linear controller.

We chose system parameters;

$$m_c = 5.0, \quad m = 0.2, \quad \ell = 2.0, \quad r = 0.5,$$
$$b = 1.5, \quad J_\phi = 0.1, \quad J_w = 0$$

and initial conditions;

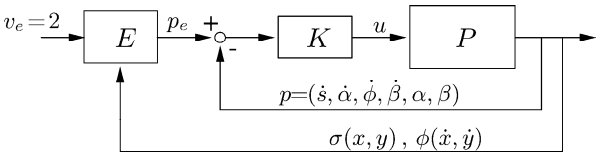

Fig. 4. Closed loop control system.

$$\dot{\alpha}(0) = \dot{\beta}(0) = \dot{s}(0) = \dot{\phi}(0) = s(0) = \alpha(0) = 0,$$
$$x(0) = 100, \quad y(0) = \dot{x}(0) = \dot{y}(0) = 0,$$
$$\beta(0) \in \{\pm 0.1, \pm 0.2\}.$$

We designated $v_e^* = 2.0$ as an independent design parameter of an equilibrium point. Then the above initial conditions give $\mu(0) = 0.01$ and (14), (20) determine other parameters $\omega_e(0) = 2v_e^*\mu(0) = 0.04$ and $\beta_e(0) = -3v_e^*\omega_e(0)/[2\ell\omega_e^2(0) + 3g] = -0.0082$ of a nominal operating point $p_e^* := [v_e^* \;\; 0 \;\; \omega_e(0) \;\; 0 \;\; 0 \;\; \beta_e(0)]$. After a linearization at that point, we designed a *LQ (Linear Quadratic)* optimal state feedback controller

$$u = \begin{bmatrix} u_s \\ u_\phi \end{bmatrix} = K[\dot{s} \;\; \dot{\alpha} \;\; \dot{\phi} \;\; \dot{\beta} \;\; \alpha \;\; \beta]^T,$$
$$K := \begin{bmatrix} -32 & -128 & 1.0 & 2.0 & -339 & 0.8 \\ 0.4 & 0.7 & 32 & 119 & -2.8 & 314 \end{bmatrix}$$

with a cost $\int_0^\infty x'Qx + u'Ru\,dt$ where $Q = diag(I_{5\times 5}, 0)$ and $R = 10^{-2} \cdot I_{2\times 2}$.

In addition, in order to induce the PPN relation (20) with time-varying $\mu(\cdot)$, the local controller K is combined with another feedback loop as shown in Fig. 4, motivated from the dual loops configuration; auto-pilot (inner) and navigation guidance (outer), in flight control. In Fig. 4, P denotes the pendulum system and the memory-less function E rebuilds new PPN-based equilibrium points at every moment subject to (14) and (20).

Note that the controller K was designed for the initial equilibrium point p_e^* solely but the operating point p_e is time-varying in the closed loop system. This observation suggests, for better performance, a gain-scheduling of a set of local controllers covering the whole equilibrium manifold Ω. This issue however is out of the range of this paper.

Our numerical simulations gave the pendulum motions shown in Fig. 5. As shown in Fig. 6, the states $\{\dot{s}, \dot{\phi}, \beta\}$ quickly approach to their limiting points in the equilibrium manifold such that satisfy the PPN relation (20) as shown in Fig. 7. Those final states, let us call them (v_f, ω_f, β_f), and arrival time t_f at the origin are given in Table 1.

Fig. 8 shows the trajectories of cart which are circular overall except some transient periods shown in Fig. 6.

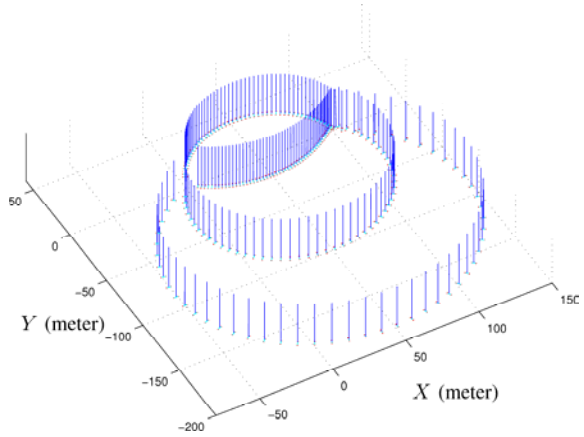

Fig. 5. Bird's-eye view of pendulum motions.

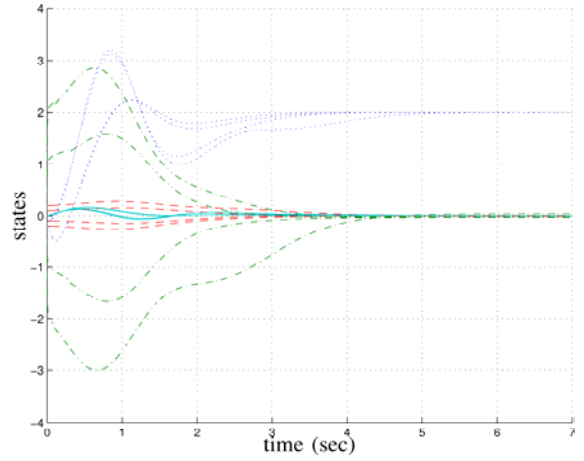

Fig. 6. State trajectories; $\dot{s}$ (dotted, meter/sec), $\dot{\phi}$ (dash-dotted, rad/sec), β (dashed, rad) and α (solid, rad).

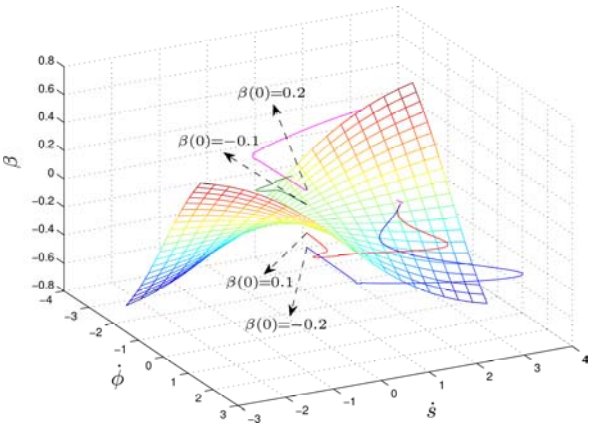

Fig. 7. Trajectories of equilibrium states.

Table 1. PPN-based equilibrium states; t_f (sec), v_f (meter/sec), ω_f (rad/sec) and β_f (rad).

$\beta(0)$	t_f	v_f	ω_f	β_f
− 0.2	262.0	2	− 0.020	+0.0041
− 0.1	53.6	2	− 0.029	+0.0059
+0.1	141.0	2	− 0.031	+0.0064
+0.2	68.2	2	+0.039	− 0.0080

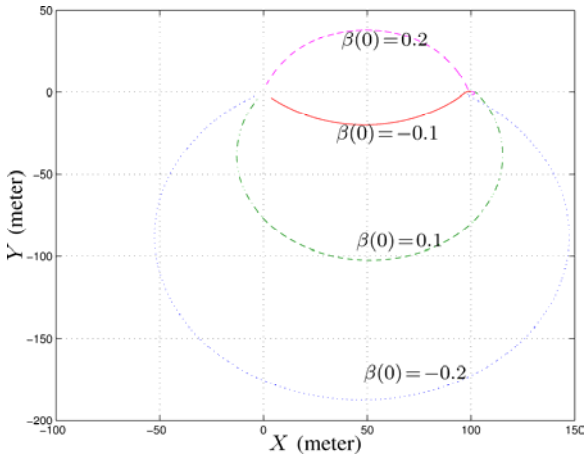

Fig. 8. Cart center trajectories.

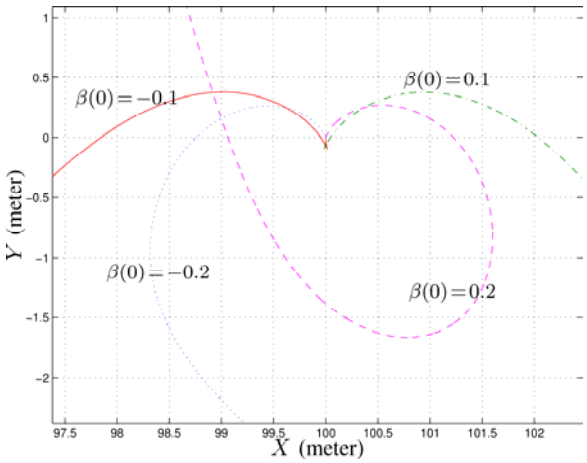

Fig. 9. Initial cart trajectories.

Notice that even though we had selected the same $v_e = 2$ for different initial angles $\beta(0) \in \{\pm 0.1, \pm 0.2\}$ at controller design stage, two steady state equilibrium parameters (ω_f, β_f) of Table 1 are determined subject to the closed loop pendulum dynamics, giving rise to four different circular trajectories shown in Fig. 8.

The initial trajectory of cart is magnified in Fig. 9. In order to physically understand those trajectories, let us note that the cart is rest at the position (100,0) facing the positive Y, call it Y+, direction initially. As an analogy, imagine a bicycle passing through the point (100,0) in Y+ direction.

Fig. 9 shows that, depending on the sign of $\beta(0)$, the cart initially makes a right or left turn, just like the above bicycle which is initially inclined to left or right trying to avoid a falling. The fact that a larger $|\beta(0)|$ gives a more sudden turning which can be seen in Fig. 9 also matches with our physical intuition.

Recall that the pendulum system is at rest initially. Thus the balancing between gravitational and centrifugal forces cannot be done until the cart gains some amount of tangential speed. Moreover it is intuitively obvious that an tangential acceleration of cart will generate not

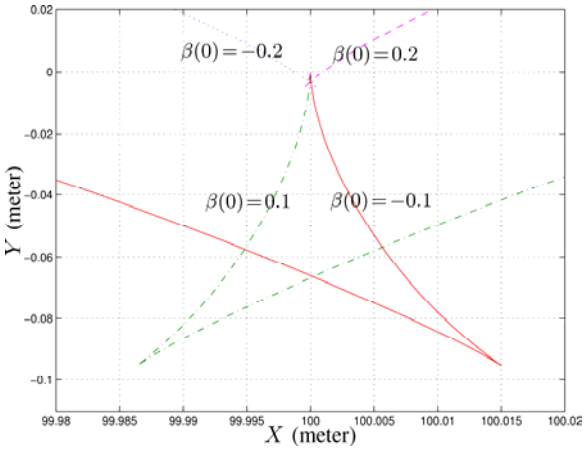

Fig. 10. Zoomed initial cart trajectories.

only the roll $\beta(\cdot)$ but the pitch $\alpha(\cdot)$ unavoidably. Those facts make the initial cart motions be more complicated than what we have observed in Fig. 9.

A second magnification of initial trajectories is shown in Fig. 10. This figure shows that initially the cart moves backward for a short period and then starts to accelerate forward. Apparently this backward motion may jeopardy the inverted pendulum but, as a reward for the risk taken, the cart can accelerate quickly avoiding unacceptable increase of the pitch angle $\alpha(\cdot)$.

It is quite surprising that our simple *linear* controller is intelligent enough to deal with such a delicate trade-off. Initial deterioration of pendulum angles caused by the backward motion are clear in Fig. 6 around 1.0 second. Returning to the bicycle analogy, this backward motion can be compared to a rider's forward lean before pushing a pedal.

5. CONCLUSION

We have developed a complete nonlinear dynamic model of a spherical inverted pendulum on a wheeled cart subject to the nonholonomic constraint of wheels and a geometric condition on the pendulum supporting point. It was shown that a linearization of the nonlinear model at a static equilibrium point results in an uncontrollable linear model and thus the existing decoupling approach for spherical pendulums cannot be used.

However a controllable linear model could be found by linearizing around a nonzero operating point near the origin. This way the spherical inverted pendulum could be stabilized with a linear controller with the limitations that inverted pendulum is not perfectly vertical but slightly inclined and that the cart need to move continuously. Furthermore by applying the proportional navigation law we have proposed a closed loop control system which can not only stabilize the inverted pendulum but also guide the cart to a desirable target position.

Numerical simulations confirmed that the linearization approach proposed in this paper works well and that even with a simple linear controller the behaviors of the closed loop system are highly complicated and very sensitive to the initial configurations.

APPENDIX A

A.1. Derivation of pendulum dynamics

The virtual work of control inputs $\{\tau_r, \tau_l\}$ can be represented as $\delta W = \tau_r \delta\theta_r + \tau_l \delta\theta_l = u_\phi \delta\phi + u_s \delta s$. In addition the Lagrange-d'Alembert equations for nonholonomic systems is given by

$$\frac{d}{dt}\left(\frac{\partial L}{\partial q_j}\right) - \frac{\partial L}{\partial q_j} = D'\lambda + Q_j, \quad j = 1, \cdots, 6,$$

where L denotes the Lagrangian and

$$D := \begin{bmatrix} \sin\phi & -\cos\phi & 0 & 0 & 0 & 0 \\ \cos\phi & \sin\phi & -1 & 0 & 0 & 0 \end{bmatrix}, \quad \lambda = \begin{bmatrix} \lambda_1 \\ \lambda_2 \end{bmatrix},$$
$$\{q_j\} := [x \quad y \quad s \quad \phi \quad \alpha \quad \beta],$$
$$Q_j := [0 \quad 0 \quad u_s \quad u_\phi \quad 0 \quad 0],$$

where the matrix D and the multipliers (λ_1, λ_2) come from the nonholonomic constraints (1)-(2). The multiplier (λ_1, λ_2) can be easily expressed by the $\{q_1, q_2\}$ components of (5) as follows

$$\begin{bmatrix} \lambda_1 \\ \lambda_2 \end{bmatrix} = \begin{bmatrix} \sin\phi & -\cos\phi \\ \cos\phi & \sin\phi \end{bmatrix} \begin{bmatrix} \frac{d}{dt}\left(\frac{\partial L}{\partial \dot{x}}\right) - \frac{\partial L}{\partial x} \\ \frac{d}{dt}\left(\frac{\partial L}{\partial \dot{y}}\right) - \frac{\partial L}{\partial y} \end{bmatrix}.$$

From this expression we obtain the reduced set of equations

$$\begin{aligned} &\frac{d}{dt}\left(\frac{\partial L}{\partial \dot{s}}\right) - \frac{\partial L}{\partial s} = -\lambda_2 + u_s, \frac{d}{dt}\left(\frac{\partial L}{\partial \dot{\phi}}\right) - \frac{\partial L}{\partial \phi} = u_\phi, \\ &\frac{d}{dt}\left(\frac{\partial L}{\partial \dot{\alpha}}\right) - \frac{\partial L}{\partial \alpha} = 0, \frac{d}{dt}\left(\frac{\partial L}{\partial \dot{\beta}}\right) - \frac{\partial L}{\partial \beta} = 0. \end{aligned} \tag{A.1}$$

Now we explicitly calculate the position $(X_\zeta, Y_\zeta, Z_\zeta)$ of the differential mass *dm* in Fig. 2 and then express the kinetic energy $K_{pen} = \frac{\rho}{2}\int_0^\ell (\dot{X}_\zeta^2 + \dot{Y}_\zeta^2 + \dot{Z}_\zeta^2)\, d\zeta$ and the potential energy $V_{pen} = \rho g \int_0^\ell Z_\zeta \, d\zeta$. From these two terms and the next kinetic energy of cart

$$K_{cart} = \frac{m_c}{2}(\dot{x}^2 + \dot{y}^2) + \frac{\tilde{J}_\phi}{2}\dot{\phi}^2 + \frac{m_w}{2}\dot{s}^2,$$

we obtain both the Lagrangian $L = K_{pen} + K_{cart} - V_{pen}$ and (A.1) in explicit form. These equations however can be simplified by making use of the relations $\ddot{s} = \ddot{x}\cos\phi + \ddot{y}\sin\phi$ and $\dot{s}\dot{\phi} = -\ddot{x}\sin\phi + \ddot{y}\cos\phi$ which come from a derivation of the nonholonomic constraints. The

resulting dynamic equations are shown in (A.2)-(A.5) and a simple rewriting gives the nonlinear dynamics (3).

$$\begin{aligned}&\frac{6(m+m_c+2m_w)}{m\ell}\ddot{s}+3\sin\beta\ddot{\phi}+3\cos\alpha\ddot{\alpha}\\&-3\sin\alpha\dot{\alpha}^2-3\sin\alpha\dot{\phi}^2+6\cos\beta\dot{\beta}\dot{\phi}\\&=\frac{6}{m\ell}u_s,\end{aligned}\tag{A.2}$$

$$\begin{aligned}&2\ell\cos\alpha\sin\beta\ddot{\alpha}-2\ell\cos\beta\sin\alpha\ddot{\beta}\\&+\ell(2-\cos2\alpha-\cos2\beta+\frac{6\tilde{J}_\phi}{m\ell^2})\ddot{\phi}+3\sin\beta\ddot{s}\\&-2\ell\sin\alpha\sin\beta\dot{\alpha}^2+2\ell\sin\alpha\sin\beta\dot{\beta}^2\\&+2\ell\sin2\alpha\dot{\alpha}\dot{\phi}+2\ell\sin2\beta\dot{\beta}\dot{\phi}+3\sin\alpha\dot{s}\dot{\phi}\\&=\frac{6}{m\ell}u_\phi,\end{aligned}\tag{A.3}$$

$$\begin{aligned}&\frac{\ell(1+\cos2\alpha)(1+\cos2\beta)}{\cos2\alpha+\cos2\beta}\ddot{\alpha}+\frac{\ell\sin2\alpha\sin2\beta}{\cos2\alpha+\cos2\beta}\ddot{\beta}\\&+2\ell\cos\alpha\sin\beta\ddot{\phi}+3\cos\alpha\ddot{s}-\ell\sin2\alpha\dot{\phi}^2\\&+\frac{\ell\sin2\alpha\sin^2 2\beta}{(\cos2\alpha+\cos2\beta)^2}\dot{\alpha}^2\\&+\frac{\ell(\cos4\beta+4\cos2\alpha\cos2\beta+3)\sin2\alpha}{2(\cos2\alpha+\cos2\beta)^2}\dot{\beta}^2\\&+\frac{2\ell\sin^2 2\alpha\sin2\beta}{(\cos2\alpha+\cos2\beta)^2}\dot{\alpha}\dot{\beta}+4\ell\cos\alpha\cos\beta\dot{\beta}\dot{\phi}\\&=\frac{3g\sin2\alpha}{\sqrt{2}\sqrt{\cos2\alpha+\cos2\beta}},\end{aligned}\tag{A.4}$$

$$\begin{aligned}&\frac{\ell\sin2\alpha\sin2\beta}{\cos2\alpha+\cos2\beta}\ddot{\alpha}+\frac{\ell(1+\cos2\alpha)(1+\cos2\beta)}{\cos2\alpha+\cos2\beta}\ddot{\beta}\\&-2\ell\cos\beta\sin\alpha\ddot{\phi}-3\cos\beta\dot{s}\dot{\phi}\\&-\ell\sin2\beta\dot{\phi}^2+\frac{\ell\sin^2 2\alpha\sin2\beta}{(\cos2\alpha+\cos2\beta)^2}\dot{\beta}^2\\&+\frac{\ell(\cos4\alpha+4\cos2\alpha\cos2\beta+3)\sin2\beta}{2(\cos2\alpha+\cos2\beta)^2}\dot{\alpha}^2\\&+\frac{2\ell\sin2\alpha\sin^2 2\beta}{(\cos2\alpha+\cos2\beta)^2}\dot{\alpha}\dot{\beta}-4\ell\cos\alpha\cos\beta\dot{\alpha}\dot{\phi}\\&=\frac{3g\sin2\beta}{\sqrt{2}\sqrt{\cos2\alpha+\cos2\beta}}.\end{aligned}\tag{A.5}$$

REFERENCES

[1] L. Consolini and M. Tosques, "On the exact tracking of the spherical inverted pendulum via an homotopy method," *System & Control Letters*, vol. 58, pp. 1-6, 2009.

[2] G. Liu, I. Mareels, and D. Nešić, "Decentralized control design of interconnected chains of integrators: a case study," *Automatica*, vol. 44, pp. 2171-2178, 2008.

[3] R. Yang, Y.-Y. Kuen, and Z. Li, "Stabilization of a 2-DOF spherical pendulum on x-y table," *Proc. of the IEEE Int. Conf. on Control Applications,* Anchorage, AK, USA, Sept. 25-27, pp. 724-729, 2000.

[4] Y. Kim, S. H. Kim, and Y. K. Kwak, "Dynamic analysis of a nonholonomic two-wheeled inverted pendulum robot," *Journal of Intelligent and Robotic Systems*, vol. 44, pp. 25-46, 2005.

[5] S. Kajita, F. Kanehiro, K. Kaneko, K. Yokoi, and H. Hirukawa, "The 3D linear inverted pendulum mode: a simple modeling for a biped walking pattern generation," *Proc. of the IEEE/RSJ Int. Conf. on Intelligent Robots and Systems*, Maui, Hawaii, USA, Oct. 29- Nov. 3, pp. 239-246, 2001.

[6] Y.-S. Ha and S. Yuta, "Trajectory tracking control for navigation of the inverse pendulum type self-contained mobile robot," *Robotics and Autonomous Systems*, vol. 17, pp. 65-80, 1996.

[7] D. Choi and J.-H. Oh, "Human-friendly motion control of a wheeled inverted pendulum by reduced-order disturbance observer," *Proc. of the IEEE Int. Conf. on Robotics and Automation*, Pasadena, CA, USA, May 19-23, pp. 2521-2526, 2008.

[8] Segway Inc., http://www.segway.com/

[9] G. Zampieri, "Nonholonomic versus vakonomic dynamics," *Journal of Differential Equations*, vol. 163, pp. 335-347, 2000.

[10] G. De Marco, "Linearization of nonholonomic systems at equilibrium points," *Rendiconti del Seminario Matematico, Universit à e Politechnico di Torino*, vol. 57, no. 3, pp. 185-195, 1999.

[11] M.-G. Yoon, "Relative circular navigation guidance for impact angle control problem," *IEEE Trans. on Aerospace and Electronic Systems*, vol. 44, no. 4, pp. 1449-1463, 2008.

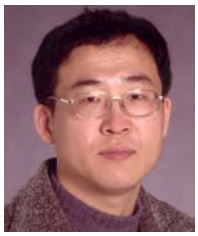

Myung-Gon Yoon was born in Cheolwon, Korea in 1967. He received the undergraduate degree in Mechanical Engineering in 1990 and his Ph.D. in Control Engineering in 1997, both from the Seoul National University, Republic of Korea. From 1999 to 2000 he was invited as a JSPS Postdoctoral Fellow at the University of Tokyo, Japan. From 2001 to 2003 he held research positions with the University of New South Wales, Australia. In 2004 he has joined the Department of Precision Mechanical Engineering, the Gangneung-Wonju National University, Korea, and he is currently an Associate Professor. His current research interests are in networked-control systems, robust control and filtering theory, guidance and nonlinear control of mechanical systems.